**RAA 2021** Vol. **21** No. **1**, 7(8pp) doi: 10.1088/1674-4527/21/1/7

*http://www.raa-journal.org* *http://iopscience.iop.org/raa*

***R**esearch in*
***A**stronomy and*
***A**strophysics*

# Photometric and spectroscopic study of flares on Ross 15

Jian-Ying Bai[1,2], Ali Esamdin[1], Xing Gao[1], Yan Yan[3,4] and Juan-Juan Ren[3]

[1] Xinjiang Astronomical Observatory, Chinese Academy of Sciences, Urumqi 830011, China; *aliyi@xao.ac.cn*
[2] University of Chinese Academy of Sciences, Beijing 100049, China
[3] National Astronomical Observatories, Chinese Academy of Sciences, Beijing 100101, China
[4] CAS Key Laboratory of Solar Activity, National Astronomical Observatories, Chinese Academy of Sciences, Beijing 100101, China

Received 2019 December 27; accepted 2020 July 10

**Abstract** We conducted photometric and spectroscopic observations of Ross 15 in order to further study the flare properties of this less observed flare star. A total of 28 $B$-band flares are detected in 128 hr of photometric observations, leading to a total flare rate of $0.22^{+0.04}_{-0.04}$ hr$^{-1}$, more accurate than that provided by previous work. We give the energy range of the $B$-band flare ($10^{29.5}$ – $10^{31.5}$ erg) and the flare frequency distribution (FFD) for the star. Within the same energy range, the FFD is lower than that of GJ 1243 (M4) and YZ CMi (M4.5), roughly in the middle of those of three M5-type stars and higher than the average FFDs of spectral types $\geq$ M6. We performed, for the first time for Ross 15, simultaneous high-cadence spectroscopic and photometric observations, resulting in detection of the most energetic flare in our sample. The intensity enhancements of the continuum and Balmer lines with significant correlations between them are detected during the flare, which is the same as those of other deeply studied flare stars with similar spectral type.

**Key words:** stars: flare — stars: activity — stars: late-type

## 1 INTRODUCTION

Flares are transient and violent phenomena occurring on the Sun and stars where a large amount of energy is released over a wide range of wavelengths, from radio to X-rays (Sanz-Forcada & Micela 2002; Osten et al. 2006; Welsh et al. 2007; Osten et al. 2010; Davenport et al. 2012). Stellar flares are considered to be triggered by magnetic reconnection in the corona (Garcia Alvarez 2000; Tamazian et al. 2005; Benz & Güdel 2010; Froning et al. 2019). Some last as short as 2 – 3 s or a few minutes, in which there exists an impulsive rise followed by a gradual exponential decay (Gershberg 1989). Therefore, using high-temporal resolution photometry and spectrometry will help to improve our understanding of their physical process (Yang et al. 2017; Honda et al. 2018; Notsu et al. 2019). Several studies have been published with photometric and simultaneous high-cadence spectroscopic observations (Lalitha et al. 2013; Kowalski et al. 2013, 2016; Froning et al. 2019).

Ross 15 is a late-type dwarf with spectral type of dM4e (Joy & Abt 1974). Recently, Muirhead et al. (2018) reported, for this star, a Vmag of 12.155±0.033 mag, a mass of 0.422 ± 0.004 $M_{\odot}$, an effective temperature of 3253 ±69 K and a radius of 0.390±0.012 $R_{\odot}$. Also, Gaia Collaboration et al. (2018) gave its distance as 76.1335±0.0541 mas (13.1348±0.0093 pc).

Ross 15 was reported as a flare-star candidate in early research (Roques 1955). Pettersen (1977) firstly studied the flare of Ross 15, reporting three flares of it through $B$ filter in 5.85 hr of observation, providing its flare rate of $0.51^{+0.29}_{-0.29}$ hr$^{-1}$. No further study related to this star has been conducted so far.

To further investigate the properties of the flares on Ross 15, in this work we conducted relatively long term photometric observations and a period of simultaneous spectral and photometric observations for this star. This paper is organized as follows. In Section 2, the observations and data reduction are outlined. In Section 3, we describe the method of data analysis for photometry and spectrometry. In Section 4, we present the results, and give discussions in Section 5. In Section 6, we provide a summary.

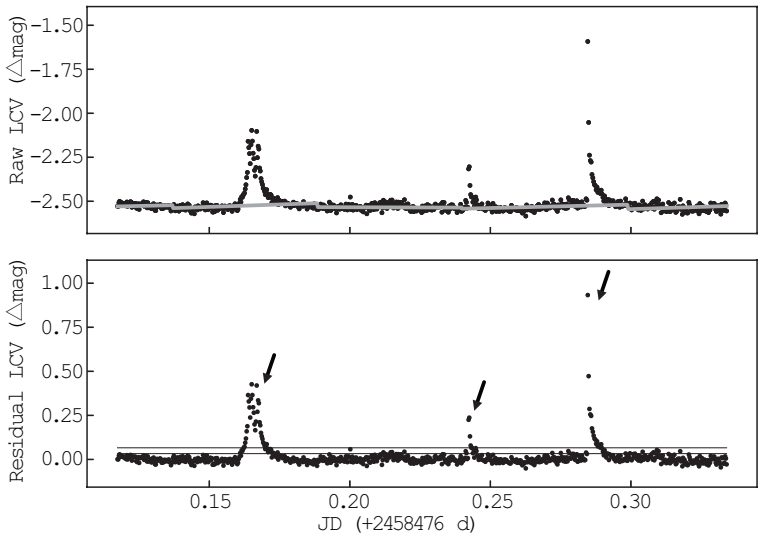


**Fig. 1** The Raw LCV and the Residual LCV on 2018 December 23. The two light curves are marked with *black points*. In the *top panel*, the *thick gray line* traces the polynomial fit of the quiescent phase. The fitting exhibits some sudden changes as we fit the quiescent phase by dividing it into several parts in order to obtain a better fitting. In the *bottom panel*, the two *black lines* indicate the positions of 2× SD (lower) and 4× SD (higher), respectively. The *arrows* also point out three identified flares.

**Table 1** Log of Photometry

| Date (UT) | Filter (Johnson) | Start (UT) | End (UT) | Duration (Hour) | Flare Number |
|---|---|---|---|---|---|
| 2018 Oct 21 | $B$ | 17:56:39 | 23:29:53 | 5.42 | 2 |
| 2018 Oct 26 | $B$ | 14:17:08 | 23:29:32 | 9.2 | 3 |
| 2018 Nov 9 | $B$ | 16:43:33 | 22:27:56 | 5.73 | 1 |
| 2018 Nov 10 | $B$ | 16:00:21 | 23:39:59 | 7.65 | 1 |
| 2018 Nov 22 | $B$ | 14:16:28 | 19:08:43 | 4.87 | 0 |
| 2018 Nov 26 | $B$ | 14:44:12 | 23:49:39 | 9.08 | 1 |
| 2018 Nov 28 | $B$ | 17:08:55 | 23:49:57 | 6.68 | 1 |
| 2018 Dec 11 | $B$ | 14:40:13 | 19:57:58 | 5.28 | 2 |
| 2018 Dec 14 | $B$ | 18:25:33 | 23:11:00 | 4.77 | 0 |
| 2018 Dec 15 | $B$ | 18:53:04 | 23:11:42 | 4.3 | 1 |
| 2018 Dec 21 | $B$ | 20:11:18 | 22:59:59 | 2.82 | 0 |
| 2018 Dec 22 | $B$ | 12:20:33 | 23:22:55 | 11.03 | 1 |
| 2018 Dec 23 | $B$ | 13:52:46 | 23:26:18 | 9.57 | 4 |
| 2018 Dec 27 | $B$ | 16:35:30 | 22:16:12 | 5.68 | 3 |
| 2019 Jan 19 | $B$ | 14:37:51 | 18:59:57 | 4.37 | 2 |
| 2019 Jan 20 | $B$ | 13:35:37 | 18:59:48 | 5.4 | 0 |
| 2019 Jan 23 | $B$ | 13:33:13 | 16:27:56 | 2.9 | 0 |
| 2019 Jan 27 | $B$ | 14:32:42 | 18:59:55 | 4.45 | 1 |
| 2019 Jan 29 | $B$ | 13:55:26 | 17:59:52 | 4.07 | 0 |
| 2019 Feb 11 | $B$ | 12:59:35 | 16:54:58 | 3.92 | 3 |
| 2019 Feb 13 | $B$ | 15:03:50 | 17:59:49 | 2.93 | 1 |
| 2019 Apr 03 | $B$ | 14:00:01 | 15:58:52 | 1.97 | 0 |
| 2019 Apr 04 | $B$ | 14:36:32 | 15:59:49 | 1.38 | 0 |
| 2019 Apr 09 | $B$ | 14:23:17 | 15:59:44 | 1.6 | 0 |
| 2019 Apr 14 | $B$ | 14:34:07 | 15:59:44 | 1.42 | 1 |
| 2019 Apr 15 | $B$ | 14:33:53 | 15:59:53 | 1.43 | 0 |

**Table 2** Log of Spectrometry

| Date (UT) | Start (UT) | End (UT) | Duration (Minute) | Flare Number |
|---|---|---|---|---|
| 2019 Feb 11 | 12:58:30 | 14:04:06 | 65 | 1 |

## 2 OBSERVATIONS AND DATA REDUCTION

### 2.1 Photometric Data

The photometric observations of Ross 15 (RA 01:59:24, Dec +58:31:16) were acquired by employing the Ningbo Bureau of Education and Xinjiang Astronomical Observatory Telescope (NEXT) facility. NEXT is located at Nanshan Station of Xinjiang Astronomical Observatory, Chinese Academy of Sciences, with an aperture of 60 cm and a focal ratio of F/8. An FLI 230-42 CCD with 2048×2048 pixels is mounted at the prime focus of the telescope, providing a field of view of 22×22 arcmin$^2$. A set of Johnson-Cousins $UBVRI$ filters is equipped for broadband photometry. The limiting magnitude of the $B$ band can reach 15.4 mag with signal-to-noise ratio (SNR) = 20 for 10 s of exposure.

We carried out the photometric observations of Ross 15 on 26 nights, ∼128 hours in total, with the $B$ filter from October, 2018 to April, 2019, utilizing NEXT. Table 1 displays the log of the photometry, including the observation date, filter used, the start and end times of each observing session, the session duration and the number of detected flares in each session. The exposure time is 10 s and the readout time is ∼15 s, leading to a ∼25 s cadence for each observing session.

The photometric data are reduced by the software MaxIm DL 5.15 with the standard procedure of bias subtraction, dark subtraction and flat field correction. The differential photometry is also performed with MaxIm DL 5.15. TYC 3696-453-1 (RA 01:59:05, Dec +58:29:09) is selected as a reference star. The formula, Error =

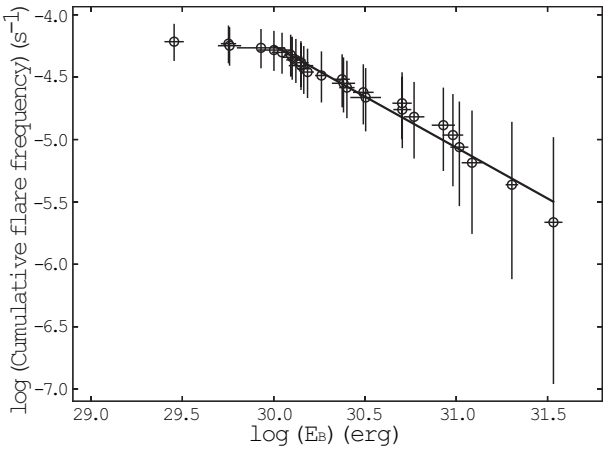


**Fig. 2** Cumulative FFD versus flare energy for the 28 events observed on Ross 15 in $B$ bandpass. The *open black circles* represent the cumulative flare frequency at each flare energy. The *vertical error bars* signify the 95% confidence intervals and the *horizontal ones* indicate the error in energy. The *black line* traces the least-squares power-law fit, $\log(\text{Flare frequency}) = -0.82^{+0.16}_{-0.16}\ \log(\text{E}_B) + 20.23^{+4.05}_{-4.05}$.

1.0857/SNR (Warner 2016), is applied to compute the photometry error in magnitude, which is the same as that of the IRAF package.

### 2.2 Spectral Data

Simultaneously with the photometric observation on 2019 February 11, the high-cadence spectra of Ross 15 were obtained by relying on a 2.16-m telescope. This telescope is located at Xinglong Station of National Astronomical Observatories, Chinese Academy of Sciences, which is equipped with the Beijing Faint Object Spectrograph and Camera (BFOSC). The wavelength coverage is from 3300 to 10 000 Å, and the resolution is $R = 1120$ at 6500 Å. The limiting magnitude of the telescope in the spectroscopic observations typically could reach $V = 20$ mag (SNR = 5) within 1 hr of exposure. More parameters of the telescope and the BFOSC can be found in Fan et al. (2016).

Table 2 presents the log of the spectrometry. The integration time is 10 s and the readout time is ∼5 s for each spectrum, leading to a ∼15 s cadence. A total of 255 spectra are obtained in 65 minutes of duration. BD+75D325 is selected as a standard star, and its spectrum is obtained with a 60 s exposure time. A total of five flat images and one Fe-Ar lamp spectrum are obtained at the beginning of the whole observation.

All the spectra are reduced with IRAF packages[1]. In order to achieve higher SNR for the spectra of Ross 15, every two spectra are combined. The combined spectra are then reduced following a standard procedure which involved zero subtraction, flat correction and spectral extraction. Wavelength and flux calibration are performed with the Fe-Ar lamp spectrum and the spectrum of the standard star, respectively.

**Table 3** Parameters of Flares

| Flare ID | $T_{\rm rise}$ (min) | $T_{\rm decay}$ (min) | $T_{\rm total}$ (min) | Amplitude (mag) | log E$_B$ |
|---|---|---|---|---|---|
| 1 | 0.73 | 3.70 | 4.43 | 0.16 ± 0.01 | 30.12 ± 0.05 |
| 2 | 0.37 | 2.20 | 2.57 | 0.06 ± 0.01 | 29.45 ± 0.05 |
| 3 | 1.07 | 8.55 | 9.62 | 0.26 ± 0.01 | 30.37 ± 0.04 |
| 4 | 11.33 | 15.35 | 26.68 | 0.27 ± 0.01 | 30.40 ± 0.04 |
| 5 | 1.07 | 6.27 | 7.33 | 0.20 ± 0.01 | 29.75 ± 0.04 |
| 6 | 0.37 | 11.22 | 11.58 | 0.35 ± 0.02 | 30.49 ± 0.06 |
| 7 | 2.53 | 9.87 | 12.40 | 0.06 ± 0.01 | 30.15 ± 0.05 |
| 8 | 1.17 | 6.23 | 7.40 | 0.38 ± 0.01 | 30.70 ± 0.05 |
| 9 | 2.98 | 6.68 | 9.67 | 0.28 ± 0.02 | 30.70 ± 0.09 |
| 10 | 0.42 | 2.97 | 3.38 | 0.08 ± 0.01 | 30.00 ± 0.03 |
| 11 | 1.23 | 2.88 | 4.12 | 0.32 ± 0.01 | 30.16 ± 0.03 |
| 12 | 1.88 | 17.23 | 19.12 | 1.21 ± 0.04 | 31.30 ± 0.13 |
| 13 | 0.85 | 1.75 | 2.60 | 0.16 ± 0.02 | 29.93 ± 0.07 |
| 14 | 1.13 | 1.10 | 2.23 | 0.16 ± 0.02 | 30.15 ± 0.06 |
| 15 | 5.50 | 11.08 | 16.58 | 0.43 ± 0.02 | 30.98 ± 0.06 |
| 16 | 0.73 | 3.68 | 4.42 | 0.24 ± 0.02 | 30.10 ± 0.06 |
| 17 | 0.45 | 9.95 | 10.40 | 0.93 ± 0.02 | 30.77 ± 0.06 |
| 18 | 1.22 | 14.63 | 15.85 | 0.96 ± 0.02 | 31.09 ± 0.06 |
| 19 | 0.75 | 1.50 | 2.25 | 0.13 ± 0.02 | 30.05 ± 0.06 |
| 20 | 0.73 | 6.07 | 6.80 | 0.12 ± 0.02 | 30.38 ± 0.06 |
| 21 | 0.87 | 1.33 | 2.20 | 0.12 ± 0.01 | 29.76 ± 0.05 |
| 22 | 0.87 | 7.85 | 8.72 | 1.04 ± 0.01 | 30.93 ± 0.05 |
| 23 | 1.28 | 8.58 | 9.87 | 0.92 ± 0.02 | 31.02 ± 0.08 |
| 24 | 4.12 | 28.42 | 32.53 | 1.07 ± 0.01 | 31.53 ± 0.03 |
| 25 | 0.83 | 10.68 | 11.52 | 0.17 ± 0.01 | 30.50 ± 0.03 |
| 26 | 0.80 | 5.35 | 6.15 | 0.17 ± 0.01 | 30.26 ± 0.03 |
| 27 | 0.43 | 1.68 | 2.12 | 0.39 ± 0.01 | 30.09 ± 0.04 |
| 28 | 0.42 | 6.03 | 6.45 | 0.23 ± 0.02 | 30.19 ± 0.06 |

## 3 DATA ANALYSIS

### 3.1 Photometric Analysis

A program has been written to detect flares from the light curve of Ross 15 on each night in an automatic manner. Through the program, in the first step, the light curve from a night (Raw LCV) is fitted iteratively by smoothing average to exclude outliers in order to obtain a quiescent phase (Hawley et al. 2014; Davenport et al. 2016; Yang et al. 2017; Yang & Liu 2019). In the second step, the quiescent phase is fitted by a polynomial fitting, and then the Raw LCV is subtracted by the polynomial fitting to get a subtracted light curve (Residual LCV). In the final step, the Residual LCV is checked to get flare candidates with similar criteria as applied in previous research (Hilton et al. 2011; Hunt-Walker et al. 2012; Hawley et al. 2014) (see Fig. 1). The criteria are as

[1] IRAF is distributed by the National Optical Astronomy Observatories (NOAO) in Tucson, Arizona, which is operated by the Association of Universities for Research in Astronomy, Inc., under cooperative agreement with the National Science Foundation.

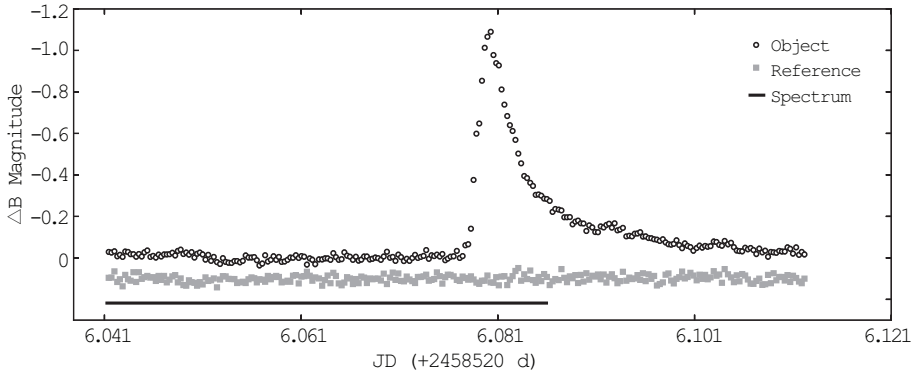


**Fig. 3** The $B$-band light curve of the 1.07-mag flare and the duration of the spectroscopic observations. The light curve of Ross 15 is marked with *open circles*. *Gray solid squares* indicate the light curve of the reference star. The $1\sigma$ errors of the photometry are less than 0.01 mag. The error bars are smaller than the sizes of the symbols in both curves. The duration of the spectrometry is marked with a *thick black line*.

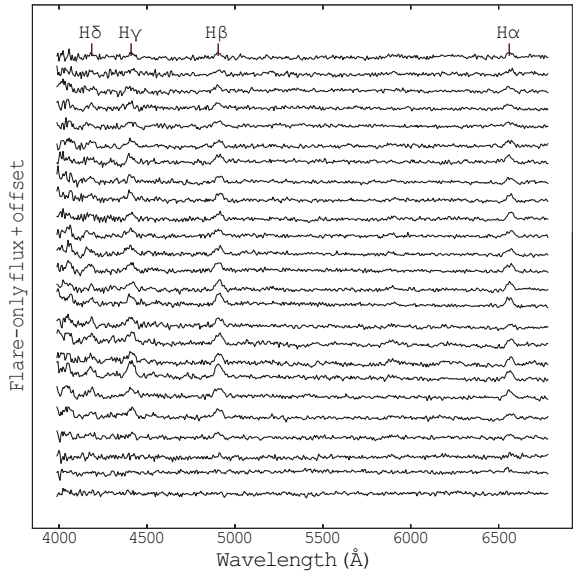


**Fig. 4** The flare-only spectra during the 1.07-mag flare. To be clear, the spectra are shifted vertically and plotted from bottom to top by the observational order. H$\alpha$, H$\beta$, H$\gamma$ and H$\delta$ emission lines are indicated on the top.

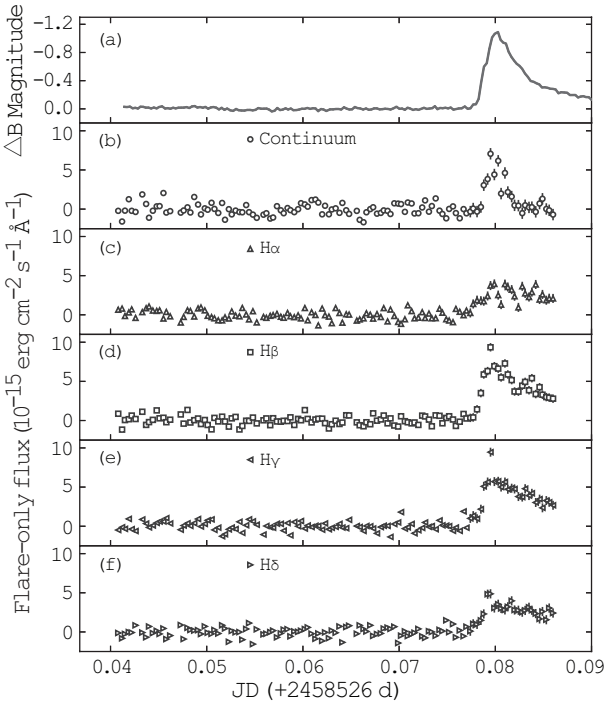


**Fig. 5** Panel (a): The light curve of the 1.07-mag flare. Panels (b) to (f): The intensity evolutions of the continuum, H$\alpha$, H$\beta$, H$\gamma$ and H$\delta$ respectively. Error bars on all panels represent the root mean square of the intensities in the pre-flare phase.

follows: (1) In a light curve of a flare, there are at least seven consecutive measurements; (2) These measurements are more than two times the standard deviation (SD) of the quiescent phase and at least one of them is more than four times the SD. Besides these two criteria, the profile of the light curve of each flare candidate is also checked through a graphical interface to confirm that the profile consists of an impulsive rise (relatively short) and an exponential decay (relatively long).

The cumulative flare frequency distribution (FFD) is a diagram of cumulative flare frequency (log number of flares per hour with energy greater than that of a flare) versus flare energy (Gershberg 1972; Lacy et al. 1976; Paudel et al. 2018). Figure 2 expresses the calculated FFD for the $B$-band flares on Ross 15 in this work. Following the method applied in Hawley et al. (2014), $B$-band flare energy is computed with the equivalent duration (Gershberg 1972) of a flare multiplied by the quiescent luminosity of the star. The equivalent duration is defined as the amount of time that the star would take in its quiescent state to release the same amount of energy released during a flare, and is calculated as the time integral of $F_f(t)/F_0$, where $F_f(t)$ is the flux of the flare and $F_0$ is the flux

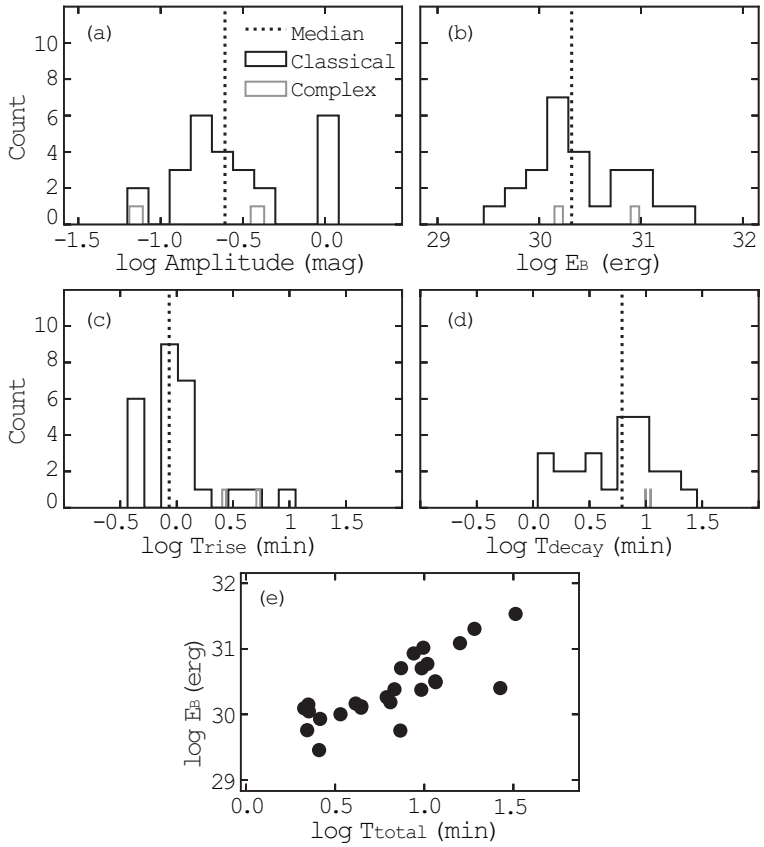


**Fig. 6** Panels (a) to (d): Histograms of flare parameters. In all the panels, the *black* and *gray lines* indicate classical and complex flares, respectively, and the *vertical dotted lines* signify the medians of the parameters of the classical flares. Panel (e): Distribution of the flare energies in $B$ band versus total durations.

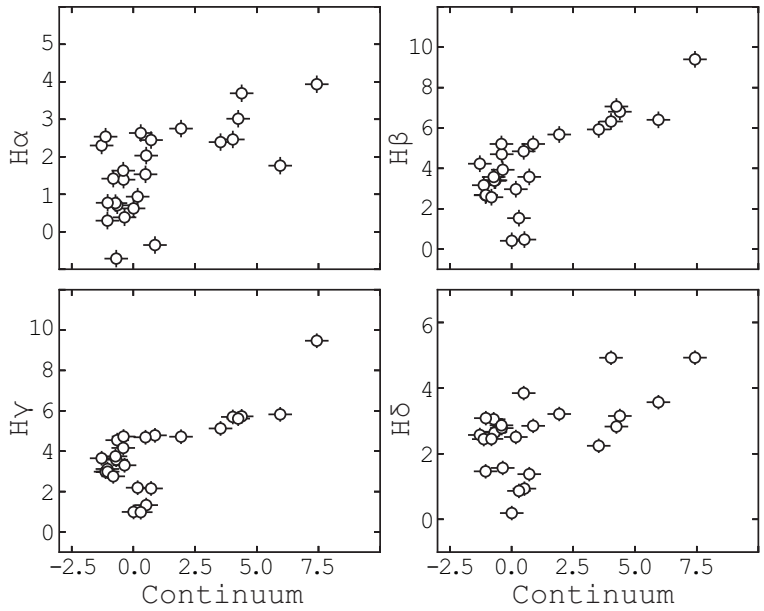


**Fig. 7** Intensity distributions between the continuum and Balmer lines during the flare phase. To be clear, all the intensity values are divided by $10^{-15}$ erg cm$^{-2}$ s$^{-1}$ Å$^{-1}$, and marked with *open circles*. The *vertical error bars* in each panel represent the standard error of the intensities of each emission line, and the horizontal ones correspond to that of the continuum.

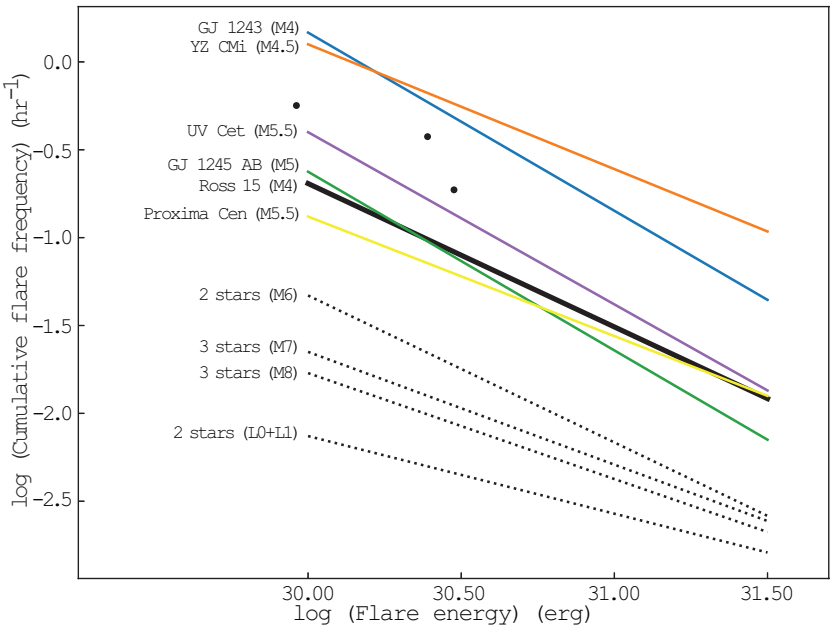


**Fig. 8** Comparison of flare rates of Ross 15 (*thick black line*) with those of GJ 1243 (M4, *blue line*), YZ CMi (M4.5, *red line*), UV Cet (M5.5, *purple line*), GJ 1245 AB (M5, *green line*), Proxima Cen (M5.5, *yellow line*) and average flare rates with different spectral types (M6 to L0+L1, *dotted lines*). The FFDs of YZ CMi and UV Cet are taken from Lacy et al. (1976), and those of GJ 1243, GJ 1245 AB and Proxima Cen are referenced from Hawley et al. (2014), Lurie et al. (2015) and Davenport et al. (2016), respectively. The average flare rates of M6 to L0+L1 are adopted from Paudel et al. (2018). Star names/numbers of stars mixed and spectral types are indicated on the left of each line. The FFD of Ross 15 in Pettersen (1977) is also plotted with *black points*.

of the star in the quiescent state (see Gershberg 1972; Hunt-Walker et al. 2012; Hawley et al. 2014). The $B$-band flux is estimated by convolving the transmission of $B$-band filter with the quiescent spectrum. Then, the quiescent luminosity in $B$ band is calculated with $4\pi d^2$ multiplied by the $B$-band flux of the quiescent state of Ross 15, where $d = 13.1348 \pm 0.0093$ pc is the distance from the star to the Earth (Gaia Collaboration et al. 2018). We estimate the quiescent luminosity of the star as $1.26 \times 10^{29}$ erg s$^{-1}$. The 95% confidence interval for flare frequency is calculated applying Poisson confidence intervals (Gehrels 1986; Davenport et al. 2016). The errors for the flare energies are computed with the errors in the photometry. For all the flares detected, we also calculated the amplitudes, the times of rise and decay, and the total duration of the flares (see Table 3).

### 3.2 Spectroscopic Analysis

One flare is detected during the simultaneous spectral and photometric observations. The photometric amplitude of the flare is up to 1.07 mag, so we note this flare as 1.07-mag flare hereafter (see Fig. 3). In this work, we define 'pre-flare' as the quiescent phase just before a flare. Intensities of emission lines and continuum are calculated to track their evolutions during the pre-flare and flare phases. All the combined spectra in the pre-flare phase are averaged to build a template. The spectra in the pre-flare and flare phases are subtracted by the template, deriving flare-only spectra (Kowalski et al. 2010), which present H$\alpha$ (6563 Å), H$\beta$ (4861 Å), H$\gamma$ (4341 Å) and H$\delta$ (4102 Å) as depicted in Figure 4. Wide wavelength ranges, 6537 – 6583 Å, 4887 – 4933 Å, 4385 – 4431 Å and 4149 – 4195 Å, are applied to calculate the intensities of H$\alpha$, H$\beta$, H$\gamma$ and H$\delta$, respectively. The range of 4218 – 4328 Å is used to obtain the intensity of the continuum. The accumulated flux in the wavelength range of the continuum or each of the emission lines in a flare-only spectrum is divided by the wavelength to get the intensity. All intensities calculated are presented in Figure 5.

## 4 RESULTS

Through the method described in Section 3.1, a total of 28 $B$-band flares are identified in the $\sim$128 hr of photometric observations, leading to a flare rate of $0.22^{+0.04}_{-0.04}$ hr$^{-1}$ through our observations. Among them, 26 flares are classical (one peak) and two are complex (two or more peaks). Table 3 gives the parameters of each flare, including the flare ID, the times of the rise and decay, the total duration of a flare, the peak amplitude in magnitude and the $B$-band energy in log. In Figure 6, panels (a) to

(d) display histograms of the amplitudes, energies, and the times of rise and decay. The median values of the four parameters are 0.25 mag, $10^{30.5}$ erg, 0.25 min and 6.2 min respectively.

Following the approach of Silverberg et al. (2016), in panel (e) of Figure 6 we show the distribution of the flare energies versus total durations. The correlation coefficient between the two parameters is 0.8. The $B$-band energy range of our detected flares is from $10^{29.5}$ to $10^{31.5}$ erg. The FFD of Ross 15 is displayed in Figure 2, and is fitted by the least-squares power law of $\log(\text{Flare frequency}) = -0.82^{+0.16}_{-0.16} \log(\text{E}_B) + 20.23^{+4.05}_{-4.05}$.

Figure 3 features the light curve of the 1.07-mag flare and the observing duration of the spectra of Ross 15. This flare is the most energetic one ($10^{31.5}$ erg) in our sample. In the observing duration, a total of 204 spectra are obtained in pre-flare phase and 51 during the flare phase, resulting in 127 combined spectra in total. In the pre-flare phase, the minimum SNR values of the combined spectra at H$\alpha$, H$\beta$, H$\gamma$ and H$\delta$ are 38, 23, 12 and 14, respectively. The intensity evolutions of the continuum and emission lines are presented in Figure 5, which exhibits significant enhancements of them during the flare. Figure 7 illustrates the distributions of the intensities of the continuum versus those of H$\alpha$, H$\beta$, H$\gamma$ and H$\delta$ during the flare phase, with correlation coefficients of 0.6, 0.8, 0.7 and 0.5, respectively.

## 5 DISCUSSION

Regarding the study of flares from Ross 15, Pettersen (1977) is the only published paper so far, in which a flare rate of $0.51^{+0.29}_{-0.29}$ hr$^{-1}$ is reported based on three $B$-band flares detected in 5.85 hr of photometric observations using a 60-cm telescope. In our work, with a telescope the same size, a more accurate $B$-band flare rate of $0.22^{+0.04}_{-0.04}$ hr$^{-1}$ is detected in 128 hr of observations. Pettersen (1977) gives a flare rate about twice that of ours, most likely due to the relatively small number of flare samples observed in a relatively short observation time, resulting in a large statistical deviation of flare rate in that work.

The relatively large number of flare samples in our work allows us to analyze the flare energy in $B$ band, especially to obtain the FFD of Ross 15. In Figure 8, within the energy range of the flares we detected, we compare the FFD of this star with those with different spectral types. M4 type includes GJ 1243 (M4) and YZ CMi (M4.5), and M5 includes UV Cet (M5.5), GJ 1245 AB (M5) and Proxima Cen (M5.5). For M6 to L0+L1, the average FFDs are computed by mixing those of targets with similar spectral types (Paudel et al. 2018). The FFDs of YZ CMi and UV Cet are reported considering $U$-band energies of flares (Lacy et al. 1976), and those of GJ 1243 and GJ 1245 AB applying Kepler energies (Hawley et al. 2014; Lurie et al. 2015). The FFD of Proxima Cen is reported adopting MOST[2] energies of flares (Davenport et al. 2016). The average flare rates of spectral types $\geq$M6 are taken from Paudel et al. (2018), which are also computed from Kepler energies of flares. As depicted in Figure 8, the flare rates of Ross 15 are lower than those of YZ CMi and GJ 1243, and approximately in the middle of those of the three M5-type stars, and higher than those with spectral types $\geq$M6. For M-type stars, the statistical results on the rotation – activity relation from several studies indicate that the stars with shorter rotation periods tend to have higher flare activity (see Lin et al. 2019; Yang & Liu 2019). The M4-type stars, YZ CMi and GJ 1243, have rapid rotation periods, 2.77729 and 0.5927$\pm$0.0002 d respectively (Hawley et al. 2014; Bychkov et al. 2017). Their rotation periods are probably shorter than that of Ross 15, resulting in higher flare rates in the FFD for them than that of our object. Figure 8 also affirms that the FFD slope of Ross 15 is comparable with those of M4 to M6 stars, and steeper than those of spectral types $\geq$M7.

Simultaneous high-cadence spectroscopic and photometric observations reveal the properties of intensity evolutions of the continuum and emission lines during the 1.07-mag flare of Ross 15. The intensities of Balmer lines (H$\alpha$, H$\beta$, H$\gamma$ and H$\delta$) are enhanced significantly during the flare. Optical wavelength observations in previous researches also show that the intensities of H$\alpha$ and H$\beta$ are enhanced during the flares of EV Lac (Melikian et al. 2006; Honda et al. 2018). The enhancements of the Balmer lines indicate that the chromospheric activities of flare stars occur in the middle chromosphere (Montes et al. 2000; Zhang 2011; Zhang et al. 2015). In addition to the Balmer lines, several studies have demonstrated that CaII H & K, NaI D and HeI lines also exhibit enhanced radiation during flares (Lalitha et al. 2013; Kowalski et al. 2013, 2016). Near- and far-ultraviolet wavelength observations with the Hubble Space Telescope affirm that the emission lines and continuum also display enhancements during the flares of GJ 1243 and GJ 674 (Kowalski et al. 2019; Froning et al. 2019).

## 6 SUMMARY

Photometric and spectroscopic observations are conducted for Ross 15. A total of 28 $B$-band flares are detected in 128-hour photometric observations, indicating a flare rate of $0.22^{+0.04}_{-0.04}$ hr$^{-1}$, more accurate than that provided

[2] The Microvariablity and Oscillations of Stars mission, whose details can be found in Walker et al. (2003).

in previous work. The energy range of the $B$-band flare ($10^{29.5}$ – $10^{31.5}$ erg) and the FFD of Ross 15 are reported for the first time. We compare the FFD with those with different spectral types in the same energy range. The comparison reveals that the FFD of Ross 15 is lower than those of GJ 1243 and YZ CMi, approximately in the middle of those of the three M5-type stars and higher than the average FFDs of spectral types $\geq$M6. Simultaneous high-cadence spectroscopic and photometric observations are performed for the first time for Ross 15, leading to detection of the most energetic flare in our sample. The intensity evolutions of the continuum and Balmer lines are tracked for the flare. Significant enhancements of intensities of the continuum and Balmer lines are manifested during the flare, and the correlation analysis indicates that there are significant correlations between them, which is the same as that of the other deeply studied flare stars with similar spectral type.

**Acknowledgements** This research is supported by the National Natural Science Foundation of China (Grant No. 11873081), and also partially supported by the Open Project Program of the Key Laboratory of Optical Astronomy, National Astronomical Observatories, CAS. We acknowledge the support of the staff of the Xinglong 2.16-m telescope.

## References

Benz, A. O., & Güdel, M. 2010, ARA&A, 48, 241
Bychkov, V. D., Bychkova, L. V., Madej, J., & Panferov, A. A. 2017, Astrophysical Bulletin, 72, 178
Davenport, J. R. A., Becker, A. C., Kowalski, A. F., et al. 2012, ApJ, 748, 58
Davenport, J. R. A., Kipping, D. M., Sasselov, D., Matthews, J. M., & Cameron, C. 2016, ApJL, 829, L31
Fan, Z., Wang, H., Jiang, X., et al. 2016, PASP, 128, 115005
Froning, C. S., Kowalski, A., France, K., et al. 2019, ApJL, 871, L26
Gaia Collaboration, Helmi, A., van Leeuwen, F., et al. 2018, VizieR Online Data Catalog, J/A+A/616/A12
Garcia Alvarez, D. 2000, Irish Astronomical Journal, 27, 117
Gehrels, N. 1986, ApJ, 303, 336
Gershberg, R. E. 1972, Ap&SS, 19, 75
Gershberg, R. E. 1989, Mem. Soc. Astron. Italiana, 60, 263
Hawley, S. L., Davenport, J. R. A., Kowalski, A. F., et al. 2014, ApJ, 797, 121
Hilton, E. J., Hawley, S. L., Kowalski, A. F., & Holtzman, J. 2011, in Astronomical Society of the Pacific Conference Series, 16th Cambridge Workshop on Cool Stars, Stellar Systems, and the Sun, 448, eds. C. Johns-Krull, M. K. Browning, & A. A. West, 197
Honda, S., Notsu, Y., Namekata, K., et al. 2018, PASJ, 70, 62
Hunt-Walker, N. M., Hilton, E. J., Kowalski, A. F., Hawley, S. L., & Matthews, J. M. 2012, PASP, 124, 545
Joy, A. H., & Abt, H. A. 1974, ApJS, 28, 1
Kowalski, A. F., Hawley, S. L., Holtzman, J. A., Wisniewski, J. P., & Hilton, E. J. 2010, ApJL, 714, L98
Kowalski, A. F., Hawley, S. L., Wisniewski, J. P., et al. 2013, ApJS, 207, 15
Kowalski, A. F., Mathioudakis, M., Hawley, S. L., et al. 2016, ApJ, 820, 95
Kowalski, A. F., Wisniewski, J. P., Hawley, S. L., et al. 2019, ApJ, 871, 167
Lacy, C. H., Moffett, T. J., & Evans, D. S. 1976, ApJS, 30, 85
Lalitha, S., Fuhrmeister, B., Wolter, U., et al. 2013, A&A, 560, A69
Lin, C. L., Ip, W. H., Hou, W. C., Huang, L. C., & Chang, H. Y. 2019, ApJ, 873, 97
Lurie, J. C., Davenport, J. R. A., Hawley, S. L., et al. 2015, ApJ, 800, 95
Melikian, N. D., Tamazian, V. S., Docobo, J. A., Karapetian, A. A., & Natsvlishvili, R. S. 2006, Astrophysics, 49, 488
Montes, D., Fernández-Figueroa, M. J., De Castro, E., et al. 2000, A&AS, 146, 103
Muirhead, P. S., Dressing, C. D., Mann, A. W., et al. 2018, VizieR Online Data Catalog, J/AJ/155/180
Notsu, Y., Maehara, H., Honda, S., et al. 2019, ApJ, 876, 58
Osten, R. A., Godet, O., Drake, S., et al. 2010, ApJ, 721, 785
Osten, R. A., Hawley, S. L., Allred, J., et al. 2006, ApJ, 647, 1349
Paudel, R. R., Gizis, J. E., Mullan, D. J., et al. 2018, ApJ, 858, 55
Pettersen, B. R. 1977, A&AS, 30, 113
Roques, P. E. 1955, PASP, 67, 34
Sanz-Forcada, J., & Micela, G. 2002, A&A, 394, 653
Silverberg, S. M., Kowalski, A. F., Davenport, J. R. A., et al. 2016, ApJ, 829, 129
Tamazian, V. S., Melikian, N. D., Karapetian, A. A., & Natsvlishvili, R. S. 2005, Astrophysics, 48, 279
Walker, G., Matthews, J., Kuschnig, R., et al. 2003, PASP, 115, 1023
Warner, B. D. D. 2016, A Practical Guide to Lightcurve Photometry and Analysis
Welsh, B. Y., Wheatley, J. M., Seibert, M., et al. 2007, ApJS, 173, 673
Yang, H., & Liu, J. 2019, ApJS, 241, 29
Yang, H., Liu, J., Gao, Q., et al. 2017, ApJ, 849, 36
Zhang, L. 2011, in Astronomical Society of the Pacific Conference Series, 9th Pacific Rim Conference on Stellar Astrophysics, 451, eds. S. Qain, K. Leung, L. Zhu, & S. Kwok, 123
Zhang, L.-Y., Pi, Q.-F., & Zhu, Z.-Z. 2015, RAA (Research in Astronomy and Astrophysics), 15, 252